# Ferroelectric Polarization of $CH_3NH_3PbI_3$: a Detailed Study Based on Density Functional Theory and Symmetry Mode Analysis

Alessandro Stroppa,[1] Claudio Quarti,[2] Filippo De Angelis,[2] and Silvia Picozzi[3]

[1]*Institute for SuPerconductors, oxides and other INnovative materials and devices, CNR-SPIN, 67100 L'Aquila, Italy**

[2]*Computational Laboratory for Hybrid/Organic Photovoltaics (CLHYO), CNR-ISTM, 06123 Perugia Italy*

[3]*CNR-SPIN, 67100 L'Aquila, Italy*

## Abstract

Ferroelectricity in halide perovskites currently represents a crucial issue, as it may have an important role for the enhancement of solar cells efficiency. Simulations of ferroelectric properties based on density functional theory are conceptually more demanding compared to "conventional" inorganic ferroelectrics, due to the presence of both organic and inorganic components in the same compound. Here we present a detailed study focused on the prototypical $CH_3NH_3PbI_3$ perovskite. By using density functional theory combined with symmetry mode analysis, we disentangle the contributions of the methylammonium cations and the role of the inorganic framework, therefore suggesting possible routes to enhance the polarization in this compound. Our estimate of the polarization is $\sim 4.42$ $\mu$C/cm$^2$, which is substantially lower than that of traditional perovskite oxides.

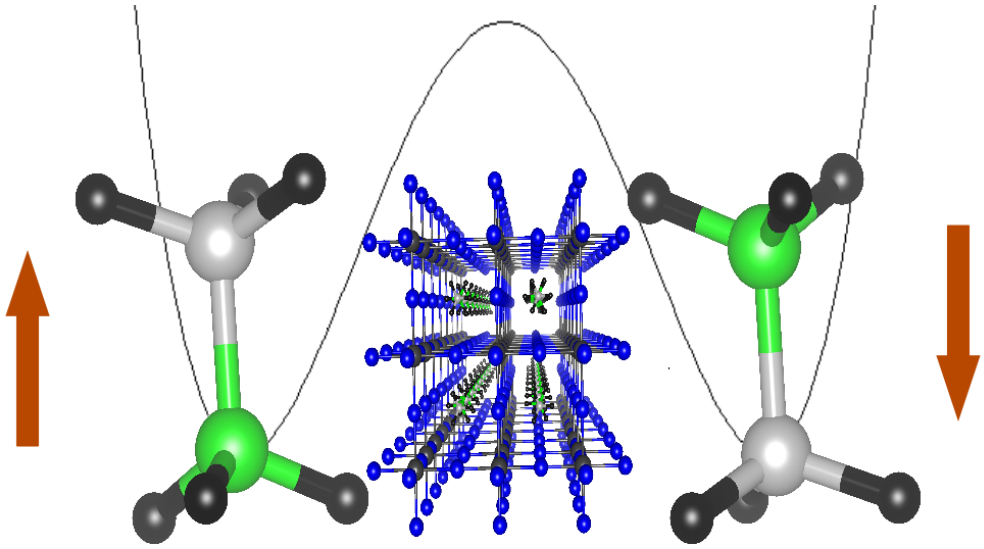

Keywords: perovskite halides, hybrid organic-inorganic materials, perovskite solar cell, ferroelectricity, photovoltaic, Lead iodide perovskite, methylammonium.

*Introduction.* In recent years, organohalide lead perovskites have represented a breakthrough in the field of photovoltaics. From their first application in 2009 by Kojima and coworkers as sensitizers in mesostructured cells,[1] showing a power conversion efficiency (PCE) of 3.81%, these materials have been widely investigated in a large variety of device configurations, ranging from mesostructured solar cells to planar heterojunction architecture.[2–11] The most performing material is $CH_3NH_3PbI_3$, that is methylammonium (MA) lead iodide, here on, named $MAPbI_3$, and its chlorine doped analogue $CH_3NH_3$ $PbI_{3-x}Cl_x$, that reached a PCE of 15% respectively in $TiO_2$ mesostructured solar cells[12] and in planar heterojunction configuration.[2] A recent paper by Zhou *et. al.* reported a PCE exceeding 19% for this material.[3] The key of the impressive PCE lies in desirable properties such as band gap $\sim$ 1.5-1.6 eV, high absorption coefficient,[1] inherent and ambipolar charge transport properties,[4,7] long carrier diffusion lengths,[5,6] small charge recombination rate,[8] together with the possibility to resort to low cost synthesis techniques for their production. Several theoretical works have addressed the electronic structure of these materials.[13–21]

A fundamental issue that has been recently discussed in the literature is the possible ferroelectricity of hybrid halide perovskites and their role on the photovoltaic performances. Interestingly, ferroelectric properties have been already shown in very similar class of compounds, *i.e.* perovskite metal-organic frameworks, both from theoretical predictions[26–28] and

confirmed by experiments.[30–32] $MAPbI_3$ shows two phase transitions, one at 327.4 K from tetragonal to cubic ($\alpha$) structure and one at 162.2 K from orthorhombic to tetragonal ($\beta$) structure.[33] The presence of the polar $CH_3NH_3^+$ cation was proposed to give rise to exotic dielectric properties.[33–36] In particular, Gesi *et al.* suggested a possible ferroelectric behavior of $MAPbI_3$[37] and Stoumpos *et al.* have first reported on the ferroelectric properties of $MAPbI_3$ by observing an hysteretic behavior in the current-voltage curve of the tetragonal $\beta$ phase of this material.[38] On the other hand, a recent work exclude the possibility of ferroelectric ordering at room temperature.[39] Frost *et al.* have theoretically investigated the ferroelectric ordering in $MAPbI_3$ perovskite with periodic Density Functional Theory (DFT) simulations.[40] Using a cubic structure where all the molecules are aligned along the same direction, they estimated a polarization of 38 $\mu C/cm^2$, *i.e.* comparable to traditional ferroelectric oxide perovskites (27 and 30 $\mu C/cm^2$ respectively for $BaTiO_3$ and $KNbO_3$).[41,42] In addition, they have also suggested a possible mechanism highlighting the key role of ferroelectricity for the photovoltaic performances in this class of materials.[43] The same authors have also investigated the possible formation of domains with a ferroelectric alignment of the MA cations as a function of temperature and of an external electric field, using a semiclassical hamiltonian.[44] However, calculations performed by Zheng *et al.* on $MAPbI_3$ and by some of the present authors on a similar hybrid halide perovskite, $CH(NH_2)_2SnI_3$, provided an estimate of the polarization of 4-5 and 5.35 $\mu C/cm^2$, respectively,[45–47] much smaller than what reported by Frost *et al.*[40] Furthermore, the tendency of $\beta$-$MAPbI_3$ to show a global alignment of the MA cations, *i.e.* a long range ferroelectric ordering of the MA cations, has been also investigated by some of us by means of DFT calculations and Car-Parrinello molecular dynamics simulations.[45] It was found that structures showing a ferroelectric order of the MA cations are the most stable ones, while structures showing an antiferroelectric alignment of the MA cations, are close in energy within a range of $k$T per $MAPbI_3$ units, and thus they are accessible at room temperature. Very recently, Kutes *et al.* have experimentally observed the presence of ferroelectric domains of the dimension of the grains (nearly 100 nm) in $\beta$-$MAPbI_3$ perovskite, by using piezoforce microscopy (PFM) on a sample prepared using a new solution-processing protocol.[48] Very recently, Liu *et al.* pointed out the importance of the ferroelectric domain walls on the photovoltaic efficiency of hybrid perovskites.[49]

Despite these preliminary studies, the specific role of ferroelectricity on the working mech-

anism of $MAPbI_3$-based solar cell has not been clarified yet and a detailed analysis of ferroelectric polarization in this class of materials is still lacking. In the present work, we performed periodic DFT simulations on the $MAPbI_3$ perovskite, focused on the evaluation of ferroelectric properties. We have found that the MA cations and their relative position within the A-site of the ideal perovskite structure play an important role for the ferroelectric polarization. If the relaxations in the $BX_3$ framework are neglected, the results can be interpreted in terms of a point charge model,[50] but have to include at least a dipole moment term to account for the non-spherical nature of organic cations. In general, the inorganic framework introduces also important structural effects which influence the final value of the polarization and, therefore, cannot be neglected in the calculations. Most importantly, our estimate of the polarization is 4.42 $\mu C/cm^2$, which is significantly lower than the one reported for standard inorganic ferroelectrics, like $BaTiO_3$ and previous calculations for $MAPbI_3$.[40]

Our results are organized as follows. First, we give a brief account of the computational details. Then we start discussing our results. Specifically, we first consider a simple model of a cubic cell containing one MA cation per unit cell, in order to have a first estimate of the polarization in $MAPbI_3$ and to easily disentangle the contributions of the MA cation and of the inorganic $BX_3$ framework. For the simple cubic case, we proceed step-by-step by adding complexity to the study: we consider the $BX_3$ framework centric and the mid point of the CN bond of the MA cation fixed at the center of the cubic cell. In this way, we provide a rough estimate of the polarization of 5.56 $\mu C/cm^2$; furthermore, in order to gain more insights in the role of the MA cation, we investigate the effect of the position of the MA cation in the cubo-octahedral cavity with respect to the $BX_3$ centrosymmetric framework. We interpret the results in terms of point charge model which suggests that, in this case, the molecular dipole, contributes negligibly to the final polarization; than we relaxed both the MA cation and the $BX_3$ framework, addressing the role of relaxations in terms of contributions of the organic/inorganic component to the final polarization. Furthermore, we analyzed the distortions of the framework by symmetry mode analysis, in order to highlight the interplay between the MA cation and the framework. We also consider different structures of the room temperature tetragonal $\beta$ phase of $MAPbI_3$ and we provide an estimation of the polarization for the most stable structure of 4.42 $\mu C/cm^2$, which is much smaller than the polarization in standard inorganic oxides. Finally we draw our conclusions.

*Computational details.* For the simple cubic case, we started our calculations from the experimental crystallographic data given in Ref. 38, optimizing the structure until Hellmann-Feynman forces were smaller than 0.02 $eV$/Å. Kohn-Sham equations were solved using the projector augmented-wave (PAW) method with the PBEsol exchange-correlation functional,[53] as implemented in VASP.[54] The energy cutoff for the plane wave expansion was set to 600 $eV$; a $8 \times 4 \times 8$ Monkhorst-Pack grid of $k$-points was used for 1×2×1 supercell. The Berry phase approach has been used to evaluate the ferroelectric polarization.[55,56] The calculation of ferroelectric polarization does not include spin-orbit interaction. Test calculations show its inclusion change the polarization by less than 0.24 $\mu C/\mathrm{cm}^2$. Details for the computational parameters used for the structures of the $\beta$ phase are given in Ref. 45. In the present work, we neglect the van der Waals interactions. In fact, we demonstrated in Ref. 45 that within the employed computational set up the inclusion of these effects does not affect the relative energetics, the shape of the crystallographic cell (*i.e.* the c/a ratio) and the orientation of the cations for a set of investigated structures.

*Results. The cubic case.* The $\alpha$-phase of $MAPbI_3$ refined at T=400 K with lattice constant $a$=$b$=6.311 Å and $c$=6.316 Å is reported in Ref. 38. If the small tetragonal distortion (about 0.07 %) is neglected, the cell is called *pseudo-cubic*, which is considered here with $a$=$b$=$c$= 6.313 Å. The center of the CN bond lies exactly at the ideal A-site position of the perovskite structure, *i.e.* at the center of the cube, with the bond aligned along the $c$-axis. We recall that the MA cation is polar, so that, upon long range ordering of MA cations, a ferroelectric (FE) polarization is to be expected along the $c$ axis. The simple cubic cell, with one MA in the unit cell, is not sufficient to evaluate the polarization, as, according to the modern theory of polarization,[55,56] a reference antiferroelectric (AFE) structure must be introduced, in terms of which the low symmetry phase can be described through symmetry breaking distortions.[28] The comparison with the AFE structure allows to monitor the spurious presence of polarization quanta, that would lead to erroneous estimates of polarization, and to analyze the atomic displacements responsible for ferroelectricity. In our case, the simplest reference structure is obtained by doubling the cubic cell along the $b$-axis, and considering the two MA cations in antiparallel and parallel orientations, that correspond respectively to the AFE and the FE arrangement (see Fig. 1 a and b). Therefore, the FE state is obtained simply by rotating one MA cation by 180° within the $bc$ plane, while the other MA cation is kept fixed. We consider step-wise rotations by 10°, *i.e.* $\theta$ from 0°

(AFE) to 180° (FE). During this "rotational path", we consider two different cases. The $BX_3$ framework is kept in centrosymmetric positions. In this way, one can perform a *functional group* analysis which allows to analyze the contributions to polarization coming from the MA cation, $P_{MA}$, while the centric $BX_3$ does not contribute; both the MA cations and $BX_3$ framework are allowed to relax: now it is possible to analyze the coupling between the MA and $BX_3$ and its effect on the final polarization.

*Centric $BX_3$ framework.* With the $BX_3$ framework being kept centrosymmetric, we have evaluated the polarization along the path from the AFE to the FE structure in Fig. 1 c. The H atoms are relaxed upon rotation of the MA cation. By construction, the polarization of the system during the "rotational path" lies in the *bc* plane. The polarization along the *c*-axis for the FE structure is 5.56 $\mu C/\mathrm{cm}^2$. The smooth variation of the polarization curve in Fig. 1 c guarantees that the present estimation is not affected by polarization quanta.

Assuming that the ammonium group $NH_3$ is positively charged the electric dipole associated to the MA cation is oriented from the carbon to the nitrogen atom *i.e.* in the same direction of the *c*-axis, see Fig. 1 b. Such assumption, based on simple chemical arguments, has been verified with quantum-chemical calculations. The Mulliken population analysis has been performed with the Gaussian09 code,[29] for the isolated MA cation, at similar level of theory used for periodic calculations (PBE/6-311G**). Such an analysis demonstrated that 62% of the positive charge of the MA cation is localized on the $NH_3$ group, in particular on the hydrogen atoms. Hirshfeld population analysis predicts a localization of the 70% of the positive charge on the $NH_3$ group. Thus, the polarization of the system lies in the same direction of MA electric dipole. Along the path, simple geometrical considerations suggest that the $P_b$ component can be expressed as $P_b=P_0 \mathrm{sen}\ \theta$, where $P_0$ is the dipole moment associated to the MA cation per unit volume, as clearly reproduced in Fig. 1 c. On the other hand, $P_c=P_0(1-\cos(\theta))=2P_0\mathrm{sen}^2(\theta/2)$. The following relation should also hold: $P_c(\theta=180)=2*P_b(\theta=90)$, almost perfectly reproduced in Fig. 1 c. When fitting the $P_0$ value from these graphs, one obtains $P_0=P_b(\theta=90)=2.67\ \mu C/\mathrm{cm}^2$. Since the $BX_3$ centric, the ionic contribution of the framework to polarisation is zero by symmetry, but its electron density can still be polarized by the dipole of the MA cation; as a result, the polarization associated to the MA cation ($P_{MA}$), 5.56 $\mu C/\mathrm{cm}^2$, inherently considers also a contribution from the polarization of the electron density of the inorganic framework.

*Point charge model and the role of molecular dipole.* We now discuss in closer detail the

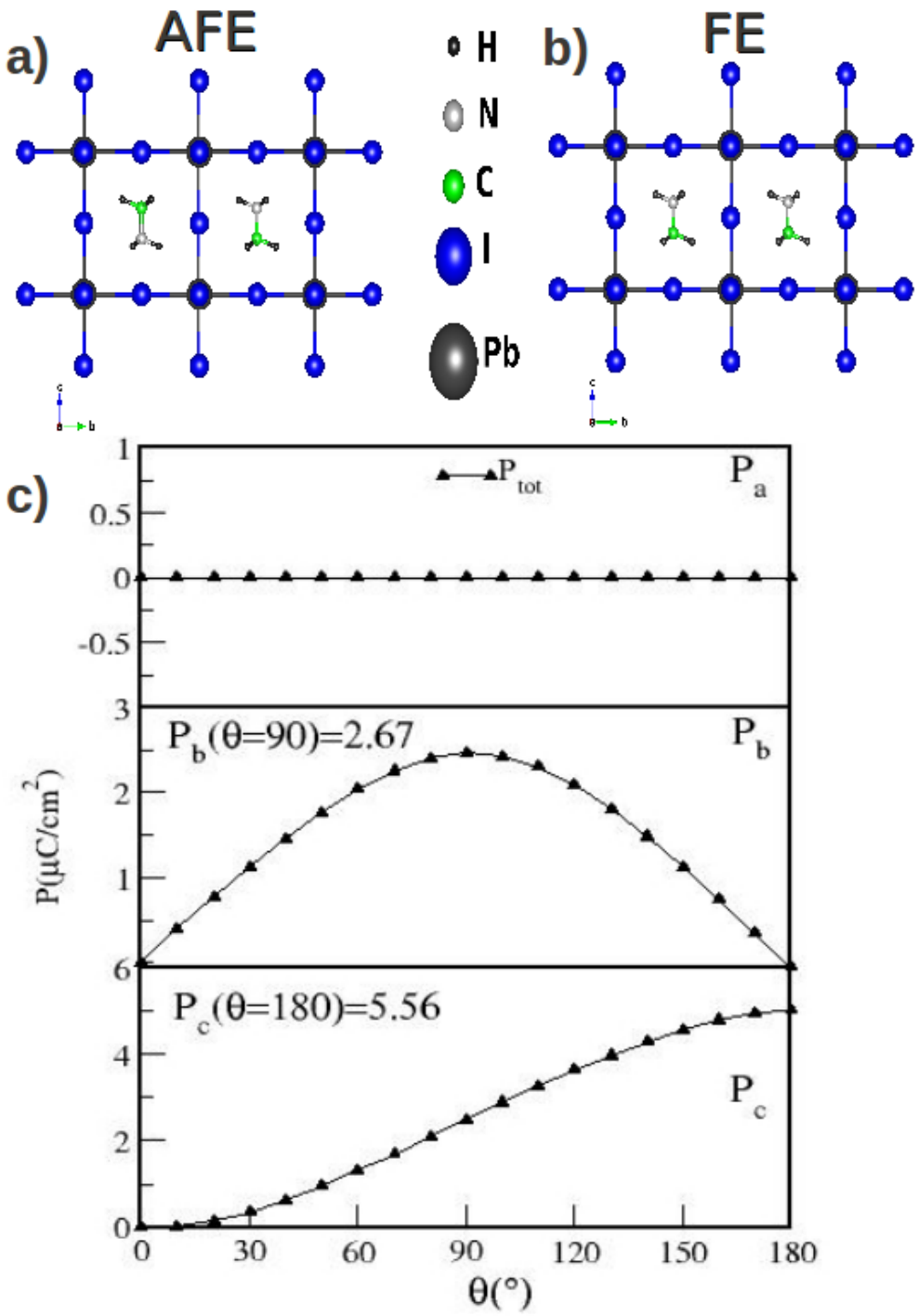


FIG. 1. a) Reference centric structure with MA cations in AFE arrangement; b) FE structure, obtained by rotating one cation by 180°; c) FE polarization along the $a$,$b$,$c$ axis.

role of the MA cation on the polarization of $MAPbI_3$. By fixing the center of the CN bond at the ideal A-site, we found a polarization P=5.56 $\mu$ C/$cm^2$ along the $c$ axis, *i.e.* parallel to

the C-N bond. However, the MA cation shows an asymmetric charge distribution, with the positive charge localized mainly on the $NH_3$ group. This is different from standard inorganic compounds, where one deals only with spherically symmetric units, *i.e.* atoms. In general, a multipole expansion of the charge distribution of MA cation gives a monopole, dipole and higher order terms. The monopole term will carry a positive charge, *i.e.* $q$=+$e$, where $e$ is the electron charge, mainly localized on the $NH_3$ group. On the other hand, the $BX_3$ centric framework has no intrinsic dipole by symmetry, but shows a monopole term carrying a negative charge, $q$=-$e$, localized by symmetry at ideal perovskite A-site which coincides with the inversion symmetry center. Thus, the polarization in the $MAPbI_3$ shows in general two contributions: an intrinsic cation electric dipole moment, $d_1$, as widely supposed in the literature[28,37,40,44] and a geometric dipole moment arising from the relative positions ($r$) of opposite charged monopole terms of the cation and the framework, say $qr$. Therefore, in a simplified picture, the polarization can be thought as P=($d_1$+$qr$)/V, where V is the volume of the unit cell. In order to disentangle these contributions, we have performed the following computational experiment. Starting from the computed Mulliken charges, we have computed a hypothetical center of charge for the MA, which lies along the CN bond, at 0.42 Å of distance from the N atom (see inset in the Figure 2). Starting with this center of charge lying exactly at the ideal A-site, we rigidly translate the MA cation along the direction of the CN bond. The results are shown in Fig. 2 a. In our reference system, a positive shift corresponds to the nitrogen moving towards the right, while a negative shift corresponds to an opposite movement. As shown in Fig. 2 a, the shift of the MA cation results in an almost linear variation of the polarization. Interestingly, when the center of charge is at the ideal A-site, the system shows a total polarization of P=($d_1$+$qr$)/V$\sim$ 2.3 $\mu$C/cm$^2$, despite the FE alignment of MA cations. Since the case with the center of charge at ideal A-site coincides with the position of the monopole term of the $BX_3$ framework, *i.e.* $r$ is equal to zero, the $qr$/V contribution is zero. It follows, that the only contribution to the polarization in this case comes from the molecular dipole of the molecule $d_1/V$, that is around 2.3 $\mu$C/cm$^2$. Note that the actual position of the charge center depends on the scheme used for the atomic population analysis, in this case the Mulliken scheme. It is likely that other population analyses may deliver different charge distributions, but their impact on the dipole polarization is expectedly small.

If the total energy is monitored as a function of the MA displacement, a minimum appears

for a displacement of $\sim$ 1.2 Å, in a configuration where the MA cation maximizes the hydrogen bond interactions with the iodine atoms. In this configuration, a final polarization of $\sim$ 11 $\mu C/\mathrm{cm}^2$ is obtained. Thus, even if the contribution of the molecular dipole to the final optimization in this case is conceptually non negligible (2.3 $\mu C/\mathrm{cm}^2$), the contribution from the monopole term is, in this case, more important.

In order to confirm our interpretation, we have carried out the same analysis by substituting the MA with a Na cation, see Fig. 2 b. It is important to note that the Na cation replacing the MA has only a role of charge balance and no relaxations have been considered for the $NaPbI_3$ system. Now, only the monopole term carried by the cation due to the spherical symmetry survives, *i.e.* $d_1$ is equal to zero. When the Na position is at ideal A-site, the polarization is zero. If the Na is displaced, the usual linear trend of the polarization is observed,[50] with almost the same slope found for the case of the MA cation (8.92 $\mu C/\mathrm{cm}^2$Å vs 8.02 $\mu C/\mathrm{cm}^2$Å). This comparison suggests that, in this case, the contribution to the polarization from the dipole of the organic MA cation gives an overall small contribution.

Finally we note that the driving force that displaces the MA cation from the ideal A-site position is due to the hydrogen bonding between the organic moiety and the inorganic framework. In fact, the formation of hydrogen bond between the $NH_3$ group of the organic cation and of the iodine atoms has been demonstrated in the literature by the analysis of structural parameters like $NH_3$ to I distance, for both static DFT and ab-initio molecular dynamic structural models.[45,51,52,58,59] In particular, recent ab-initio molecular dynamic investigations suggested the transition from the cubic to the tetragonal structure being associated to a transition between a phase with nearly rotating molecules to a phase with molecules jumping from one direction with a strong hydrogen bond network to another.[52] Therefore, there are two possible routes to tune ferroelectricity in $MAPbI_3$: either one can act directly on the A-site, by atom substitution, in order to increase the dipole term of the organic cation, as initially suggested in the context of perovskite metal-organic framework,[28] and recently applied to perovskite halides;[44] or one can fine control the hydrogen bonding network, for instance, by substituting the iodine with more electronegative atoms in selected positions.

*Relaxations of framework and organic cation.* We now consider the case where the $BX_3$ and the MA cation are allowed to relax. First, we fully relax the FE cubic structure of $MAPbI_3$ and then we consider a path between this one and the AFE structure used before.

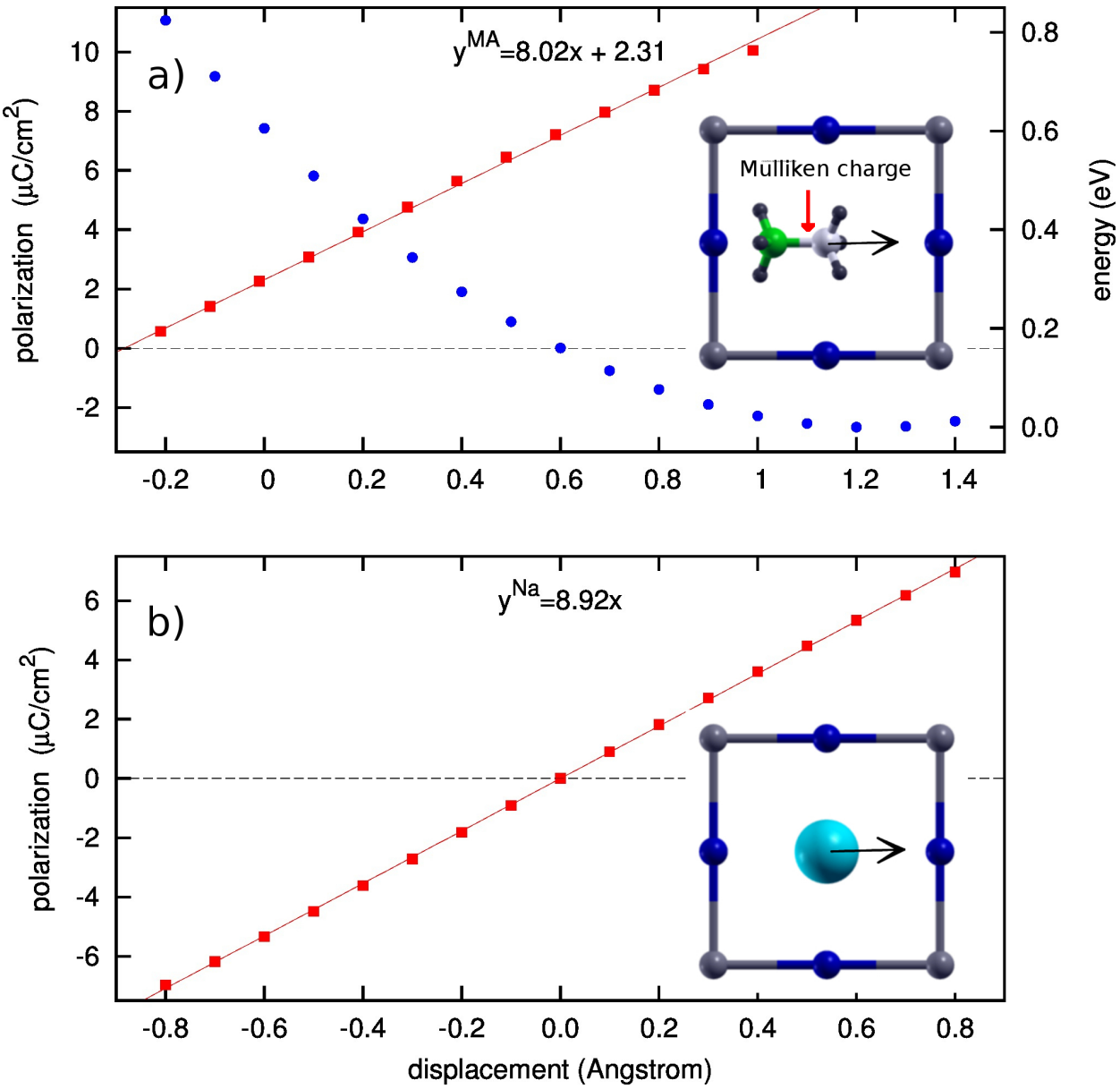


FIG. 2. a) Polarization of the cubic model (inorganic atoms fixed in cubic positions) as a function of the displacement of the MA cation from the center of the cell along the direction of the CN axis. In zero, the center of charge calculated from the Mulliken population analysis lies at the center of the cell (ideal A-site). Positive/negative values of the displacement refer to rigid shift of the MA from the center; together with the polarization, we report the energy of the system. b) same as a) but with the MA substituted by a Na cation and only the polarization is shown.

The polarization along the path from the AFE to the relaxed FE system is reported in Fig. 3. The coupling of MA cations with the framework via hydrogen bonding induces, on one

hand, a shift and tilting of the MA cation within the cubo-octahedral cavity and, on the other hand, the distortions of the inorganic framework. As a result of atomic relaxations, the polarization largely increases, up to a final value of $\sim$ (0,−3.45,13.37) $\mu C/\mathrm{cm}^2$. Interestingly, a $P_b$ component orthogonal to the main alignment of the MA cation arises, due to both the tilting of the MA cation with respect to the $c$ axis and to the distortions of the framework which reduce the I-Pb-I angles with respect to the ideal 180° value. Since the

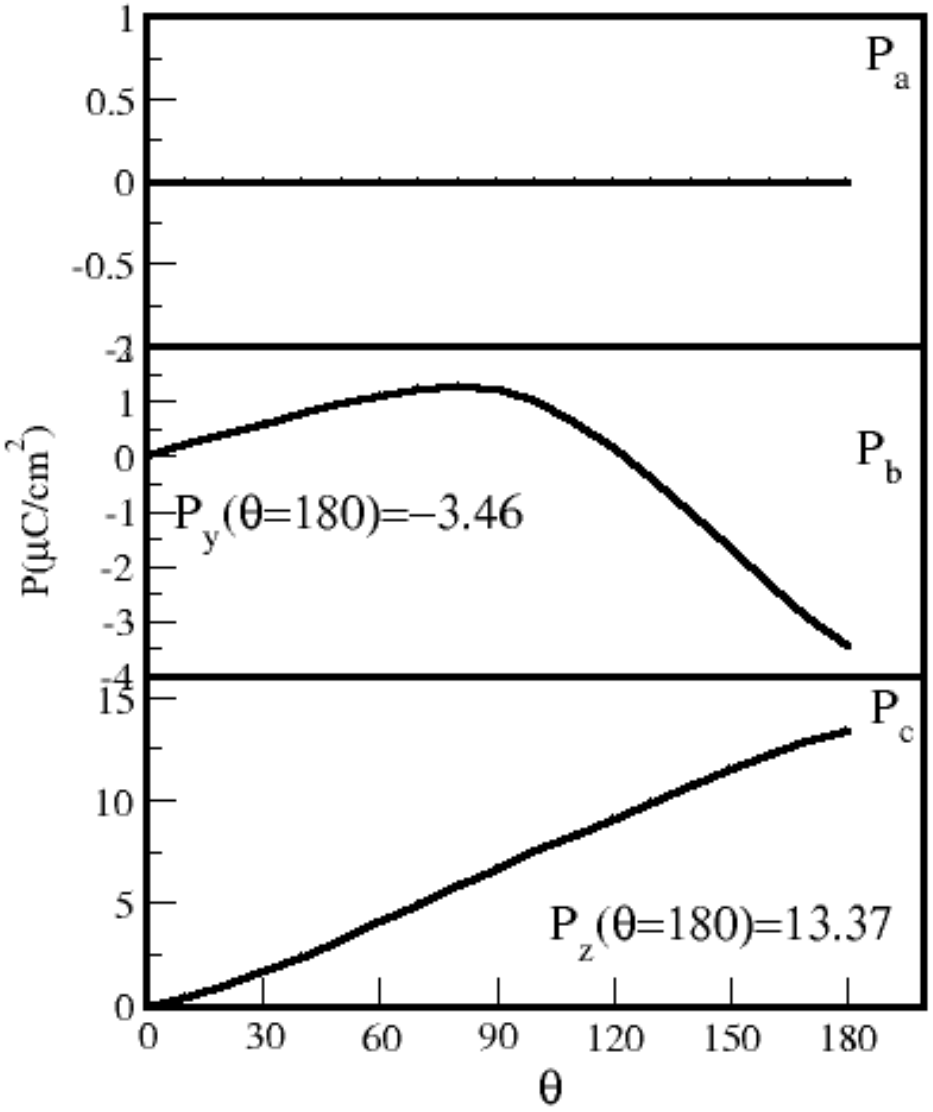


FIG. 3. Polarization of the cubic model, with all atoms allowed to relax. The upper, central and lower panels show the polarization components along $a$, $b$ and $c$, respectively.

electronegativity of Pb and I are 2.33 and 2.66 respectively, the Pb-I bonds are slightly polar. These structural relaxations leave uncompensated dipoles, both parallel and perpendicular to the MA direction.

Note that the space group for the relaxed unit cell is $Pm$. This space group allows a monoclinic axis along $a$ in our case and a mirror plane perpendicular to it. The polarization is allowed on the plane perpendicular (mirror plane) to the monoclinic axis. Therefore, according to symmetry arguments, one would expect the polarization in the $bc$ plane, in excellent agreement with our *ab*-initio calculations.

Finally, in order to disentangle the contribution of MA and $BX_3$ to the total polarization, we have again replaced the MA cation with a Na cation at the ideal cubic position, keeping the $BX_3$ relaxed positions as in fully relaxed $MAPbI_3$. Since the Na atoms occupy the A-site, they do not carry contribution to the FE polarization. For the $NaPbI_3$ system, we obtain a polarization of (0,-2.88,8.11) $\mu C/\text{cm}^2$, that corresponds to the contribution from the inorganic $BX_3$ framework, *i.e.* $P \sim P_{BX_3}$. It is now interesting to compare with the previous case, when the $BX_3$ was centric. Clearly, the relaxation of the $BX_3$ is the main responsible for the appearance of the $P_b$ component, *i.e.* perpendicular to the MA dipole moment. On the other hand, $P_c$ in $NaPbI_3$ is smaller than $P_c$ in fully relaxed $MAPbI_3$. In particular, $P_c(MAPbI_3) \sim P_c(NaPbI_3) + P_{MA} \sim P_c(NaPbI_3) + 5.56\ \mu C/\text{cm}^2$. Therefore, the relaxations of the framework induce a polarization component both perpendicular and parallel to the C-N dipole, where the parallel component is even larger than the contribution carried by the MA cation. This suggests that, in principle, the $BX_3$ contributions cannot be neglected in the evaluation of the FE polarization and that the use of different halogen atoms, *i.e.* changing the polarizability of the $BX_3$, may introduce an additional degree of freedom in tuning the FE polarization.

Finally, we analyze the atomic displacements by symmetry mode analysis. Since we want to focus on the role of the framework, as before, we replace MA with Na at ideal perovskite structure. The space group of $NaPbI_3$ is pseudosymmetric to a centric $Pm\bar{3}m$ space group of the inorganic $ABX_3$ perovskite. Since there exists a group-subgroup relation, it is possible to express the high-symmetry phase using the subgroup basis. After establishing a one-to-one map between the atomic positions of the two phases, we calculate the atomic displacements connecting the centric structure to the distorted one. The collective atomic displacements have a maximum amplitude of 0.72 Å and they can be classified according to two symmetry

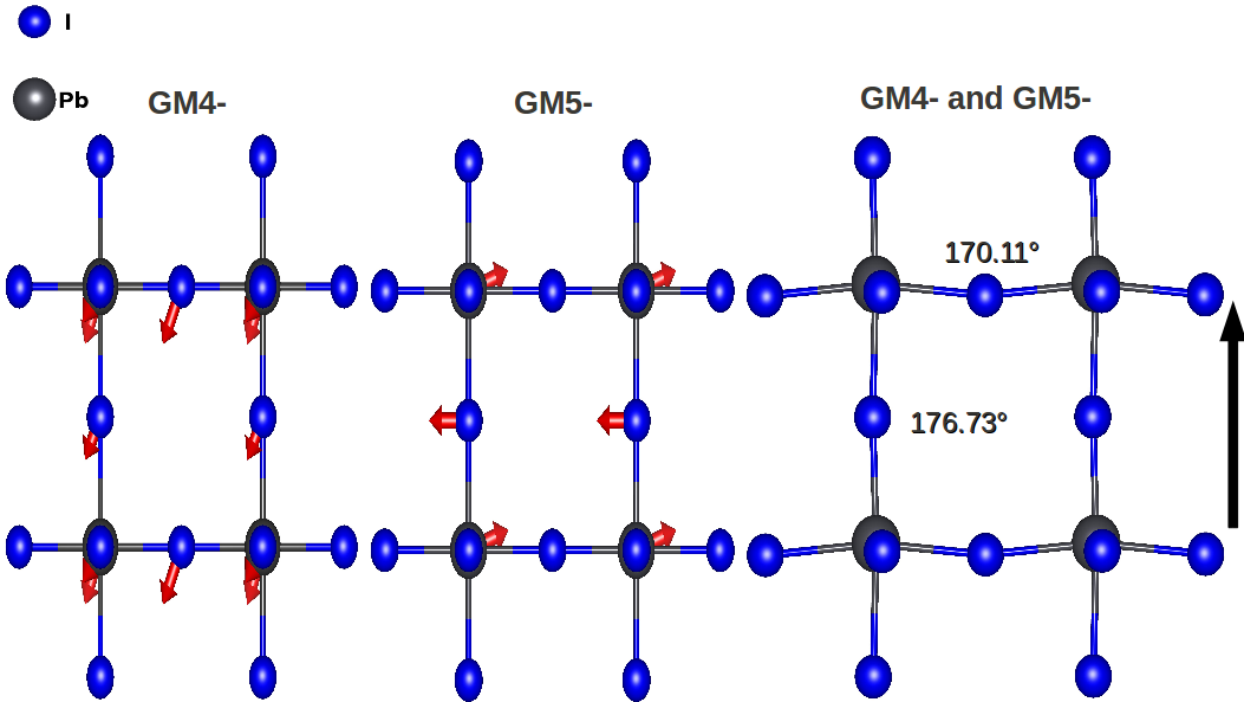


FIG. 4. Symmetry mode analysis of atomic displacements of $BX_3$ induced by the rotations on the MA cations. From left to right: GM4-, GM5- symmetry modes and resulting distortions on the framework with bending of the I-Pb-I bonds. The absolute values of the displacements are from 0.57 to 0.72 Å for I, and $\sim$ 0.48 Å for Pb.

modes such as GM5- and GM4-. The former acts only on the I atoms, while the latter acts on both Pb and I atoms. Both modes have isotropy subgroup $Pm$, *i.e.* both of them break inversion symmetry thus confirming that the $BX_3$ indeed contributes to polarization. In Fig. 4 we show the atomic displacements for both distortion modes with respect to ideal centric structure. The atomic displacements are mainly localized on iodine atoms and they are responsible for the bending of the I-Pb-I bonds, with deviations from the ideal 180 by $\sim$ 3° and $\sim$ 10°. This bending, in turn, leaves uncompensated dipoles along the C-N direction, (shown by black arrow), as well as perpendicular to it. In particular, the larger (smaller) bendings correlate with uncompensated Pb-I dipoles parallel (perpendicular) to MA cations.

In summary, a final polarization value of $\sim$ 13.37 $\mu C/\mathrm{cm}^2$ is reported for the cubic $MAPbI_3$ system. Our estimate is much smaller than that provided by Frost *et. al.* (38 $\mu C/\mathrm{cm}^2$)[40] for the same reference system. The discrepancy with the previous study[40] may be possibly due to the neglect of the relaxations and/or the possible inclusion of polarization

quanta in Ref. 40.

*The $\beta$ phase of $MAPbI_3$.* Here, we report the polarization of $MAPbI_3$ by considering realistic DFT structures for the $\beta$ phase,[57–60] as investigated in Ref. 45 where different guess structures characterized by different orientations of the MA cations, and their relative stability and evolution at room temperature, have been investigated by static DFT calculations and Car-Parrinello molecular dynamics simulations.[45] Here, we evaluate the polarization of the three structures reported in Fig. 5 a, b and c, optimized at the DFT level.[45] They correspond to a $\sqrt{2} \times \sqrt{2} \times 2$ supercell with respect to the simple cubic.

The structure in Fig. 5 a, here on named structure **a**, is the most stable structure. The MA cations are FE coupled within planes perpendicular to $c$ axis and they are tilted by 36° with respect to the $ab$ plane showing a preferential alignment along the $c$-axis, while there is no preferential alignment within the $ab$ plane. Therefore, structure **a** shows a net polarization along the $c$-axis as a result of the tilting of the MA dipole moments, *i.e.* it is a weak-ferroelectric. As already pointed out in Ref. 28, the presence of weak-ferroelectricity is not unusual in hybrid-organic compounds, at variance with standard inorganic compounds, where it is a rare phenomenon. It is worth to note that this structure is in very good agreement with the structure recently proposed by Weller *et al.* from neutron diffraction measurements for the tetragonal phase at low (180 K) temperature.[61] The structure shown in Fig. 5 b, here on named structure **b**, has MA dipoles AFE coupled within plane perpendicular to the $c$ axis, they are tilted with respect to the $ab$ plane. Therefore, structure **b** is expected to show negligible polarization in all the crystalline directions. This structure lies just 23 meV per $MAPbI_3$ unit higher in energy with respect to structure **a**. Finally, the structure shown in Fig. 5 c, here on named structure **c**, has all molecules oriented in the direction of the $c$-axis. Although it may be described by using a simple cubic cell as discussed before, we considered it again in order to consistently compare the total energies of the different structures using the same unit cell. Structure **c** is very unstable, lying 117 meV per $MAPbI_3$ unit higher in energy than structure **b** one, but it is considered here as an upper limit of the polarization for $MAPbI_3$.

To evaluate the polarization of the three structures in Fig. 5 a, b and c, we followed the same procedure outlined for the cubic phase, defining an AFE reference structure used to describe the three structures of interest. The AFE reference phase has been obtained by centrosymmetrizing the $BX_3$ framework and by imposing the same inversion center of the

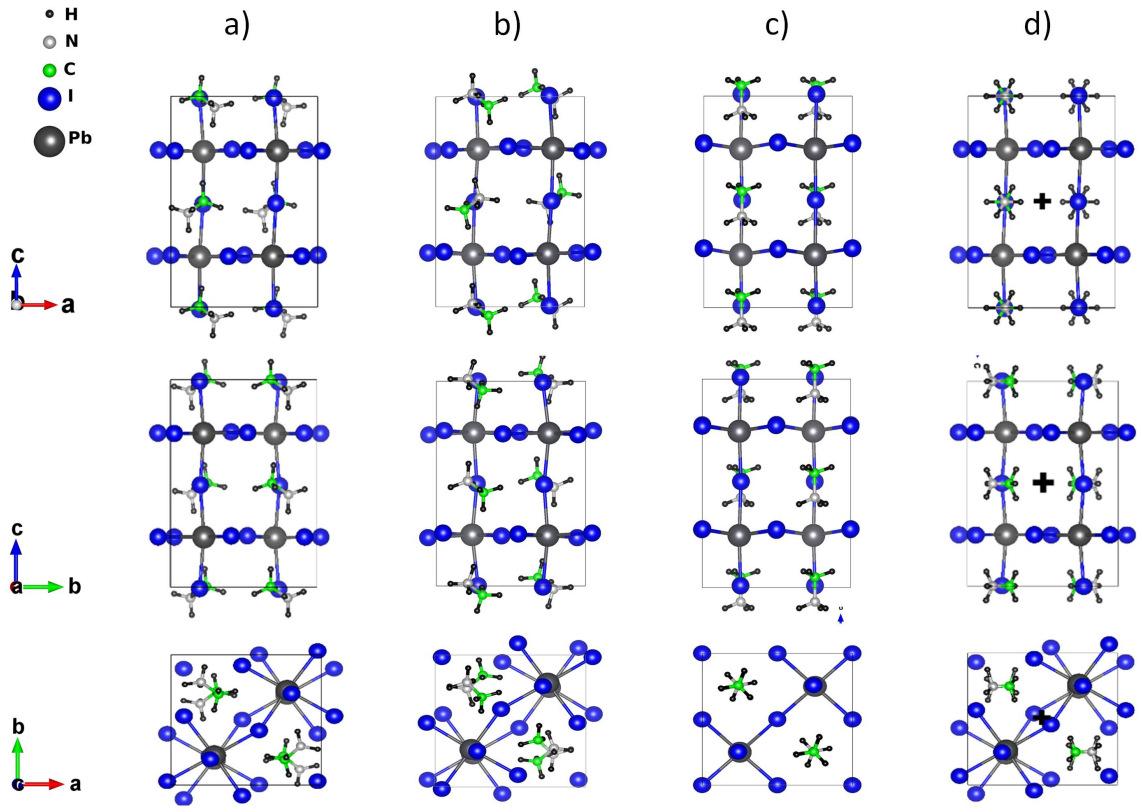


FIG. 5. Reference structures used to evaluate the polarization of the $MAPbI_3$ perovskite. a, b, and c shows respectively structure **a**,**b**,**c** used to estimate the polarization; **d** depicts the reference AFE structure, with the black cross showing the inversion symmetry center.

framework to the MA organic cations as depicted in Fig. 5 d by a black cross. In the centric structure, the MA cations are parallel to the $a$-axis forming FE alignment in a plane parallel to $bc$ plane, which is coupled AFE with next plane along the $a$ axis (see Fig. 5 b).

We now focus on the most stable structure, *i.e.* structure **a**, for which we give a detailed analysis. We estimate a polarization of $P_a \sim P_b \sim 0$, while $P_c$=−4.42 $\mu C/cm^2$. It is interesting to evaluate the contribution $P_{MA}$ and $P_{BX_3}$. As before, for $P_{BX_3}$ we considered the substitution of $MA$ with Na at ideal A-site, but keeping the $BX_3$ positions of the relaxed structure **a**. For $P_{MA}$ we consider centric $BX_3$ framework. For $P_{BX_3}$ we obtain (−2.04,3.10,0.23) $\mu C/cm^2$ while for $P_{MA}$ we obtain (2.60,−3.28, −4.47) $\mu C/cm^2$. Interestingly, $P_{MA}$+$P_{BX_3}$∼(0.56,−0.18,−4.24) is very close to P evaluated by considering the

distortions of both the organic cation and the framework. This result demonstrates, on one hand, the main role of the MA cations on the polarization of the $MAPbI_3$ for the tetragonal phase and, on the other, it points out the additivity of the polarization contributions from the different functional units, such as organic cations and framework.

Finally we analyze the atomic displacements with respect to the reference centric phase. We focus on atomic displacements of the inorganic component, thus we consider $NaPbX_3$ with the framework frozen at the relaxed atomic positions of structure **a**. In Fig. 6 we show the centric reference structure and the atomic displacement field as vectors. The displacement field can be decomposed according to two symmetrized modes: GM1+ and GM1-. The former keeps inversion symmetry but it introduces large atomic displacements for both Pb and I atoms responsible for the bending of the Pb-I-Pb. In particular the displacements are $\sim$ 0.2-0.3 Å for I and 0.03-0.06 Å for Pb. The bond angle is now $\sim 155°$. Furthermore, the 6 Pb-I bond length's initially equal to 3.130 Å, are now distorted leading to six different bond length's, *i.e.* 3.145,3.220,3.175,3.180,3.186,3.271 Å. Since the Pb-I bonds are polar with different lengths, this leaves an uncompensated dipole moment associated to each perovskite unit. Therefore, the GM1+ forces an AFE arrangement of octahedra dipole moments. The GM1- breaks the inversion symmetry with atomic displacements mainly in the *ab* plane. The displacements are $\sim$ 0.1-0.2 Å for Pb and I and they further affects the Pb-I bond lengths, thus leaving an uncompensated dipole moment in the unit cell which accounts for the estimated $P_{BX_3}$. The GM1- is clearly responsible for the contribution to the polarization in the *ab* plane. As last note, we notice that the present calculations neglects the contribution on the polarization due to the van der Waals interactions, which some recent studies pointed out being important for the correct prediction of the crystalline structure of the $MAPbI_3$ perovskite.[23] To investigate this point, we have re-optimized the structure **a** including the van der Waals interactions through the Grimme DFT-D approach,[62] and then we have calculated the polarization from the paraelectric structure **d** to the new structure **a**, following the well known modern theory of the polarization.[55,56] We found that the value of the polarization with the van der Waals interactions is -4.37 $\mu C/cm^2$, that is the nearly the same than without the van der Waals interactions. On the other hand, such result is not unexpected. In fact, in Ref. 45 we had already pointed out the limited effect of van der Waals interactions for the $MAPbI_3$ perovskite, with respect to the energetics, the crystallographic shape (the c/a ratio) and orientation of the molecules. For instance, consider that the tilting

of the molecule in the "a" structure with respect to the crystallographic $ab$-plane is decreased on the average by only 1 degree. For structure **b**, a final polarization of $\sim 0$ $\mu C/\mathrm{cm}^2$ along

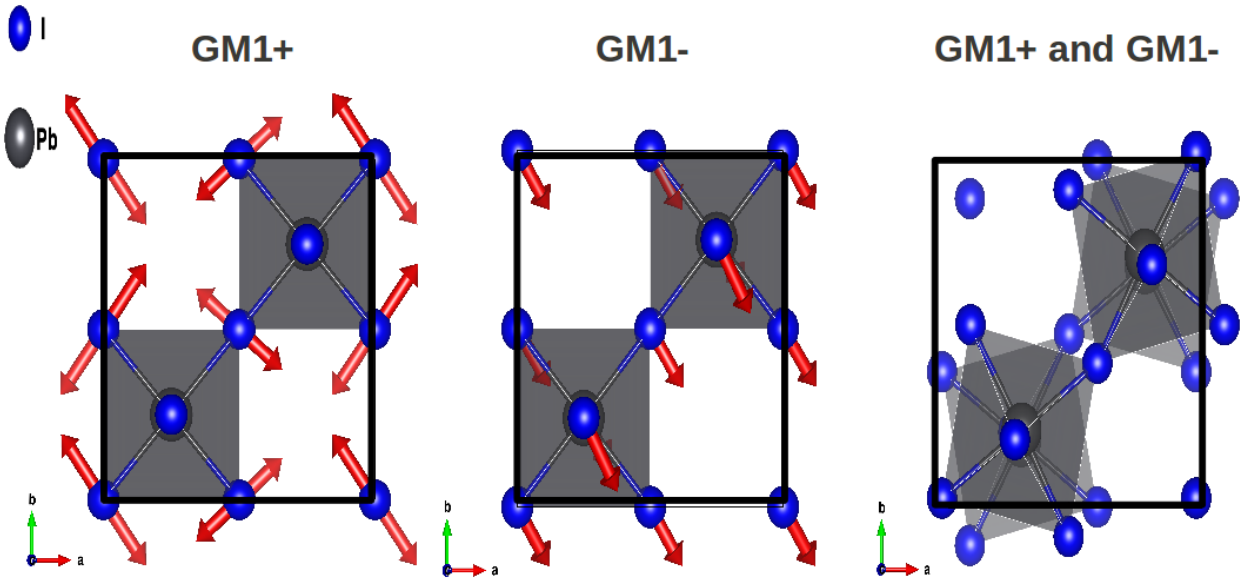


FIG. 6. Symmetry mode analysis of atomic displacements of $BX_3$ induced by the rotations on the MA cations. From left to right: GM1+ fully symmetric mode which preserves inversion symmetry but introduces large bending in the Pb-I-Pb bonds; GM1- symmetry mode responsible for the loss of the inversion symmetry and $BX_3$ polarization in the $ab$ plane; combined effect of the GM1+ and GM1- modes giving the final distortions of the framework.

all the three crystallographic axes and thus we confirm that the present structure is nearly AFE. This result is interesting, since, although structure **a** is the most stable one, structure **b** lies just at 23 meV (per $MAPbI_3$ unit) higher in energy and therefore it is accessible at room temperature. We now focus on structure **c**. The present structure should provide an upper value for the polarization for the $\beta$ phase of $MAPbI_3$ since the MA cations are all oriented in the same direction. The final polarization for this structure is $\sim 0$ along both the $a$ and $b$-axes, while it is estimated as 13.21 $\mu C/\mathrm{cm}^2$ along the c-axis. This value well compare with our previous estimate. Note, once again, that the present upper limit to the polarization for the $MAPbI_3$ perovskite is much smaller than the polarization for traditional inorganic oxide perovskites.

*Conclusions.* Methylammonium lead iodide perovskite, $MAPbI_3$, has recently emerged as a very promising candidate for photovoltaic applications, although there are still many open questions about its basics photophysical properties. In particular, a FE behavior has been observed for these materials,[38] but an in-depth theoretical investigation of the polarization properties of this class of materials was still lacking. By combining density functional theory and symmetry mode analysis, we present a study of the FE polarization of the $MAPbI_3$ hybrid perovskite. We first discussed the ferroelectricity of $MAPbI_3$ for the simple cubic model. We have disentangled the contribution of organic MA cations and of the inorganic framework to the total polarization. We have shown that the organic MA cation plays an important role in determining the final polarization. However, such a contribution does not arise by its permanent dipole moment, but from the relative position of the MA cation with respect to the inorganic framework within the A-site cavity.

We have also verified that the contribution due to the relaxations of the inorganic framework to the polarization is, in principle, comparable to that due to the organic component, and, therefore, must be taken into account for a reliable estimate of the polarization. The effect of the framework is stronger when the MA dipoles are aligned collinearly, which can be simulated using a simple cubic cell. These results thus point out the importance of hydrogen bonds between organic cations and iodine atoms on the polarization properties of hybrid lead halide perovskites and they suggest possible routes to tune the FE properties by acting on the formation of strong and ordered hydrogen bond network through proper modifications of the $BX_3$ framework, *e.g.* halogen atom substitutions.

Moreover, we provided an accurate estimate of the polarization of the room temperature tetragonal phase, considering three structures, characterized by different relative orientations of the MA cations. The most stable structure, structure **a**, has a final polarization of 4.42 $\mu C/\mathrm{cm}^2$, that is much smaller than the polarization of inorganic oxide perovskites, as $BaTiO_3$ (27 $\mu C/\mathrm{cm}^2$). The structure shows the presence of weak-ferroelectric polarization, *i.e.* the organic dipole moments are slightly tilted (around 30) with respect to a reference axis, giving rise to an uncompensated dipole. In this regard, an upper value for the polarization of 13.21 $\mu C/\mathrm{cm}^2$ is estimated for the structure with the maximum alignment of the MA cations. Such a structure however lies very high in energy with respect to the most stable weak-ferroelectric structure (nearly 0.5 eV) and it could thus be accessible only in extreme conditions, as, for instance under the application of an external field.

Finally, it is worth to discuss briefly on the effect on the polarization of the dynamic effects, associated to the thermal motion at room temperature. Our estimation of 4.42 $\mu C/\mathrm{cm}^2$ for the polarization inherently assumes that no orientational motion for the MA cations is present. In this sense, 4.42 $\mu C/\mathrm{cm}^2$ could be representative of the structure measured by Weller et. al., for the tetragonal phase of $MAPbI_3$ at 180 K,[61] that is in extremely good agreement with our computed structure. However, at higher temperature, the thermal motion of the MA cations is expected to decrease the alignment of the MA cations in the perovskite, thus to decrease the polarization. Consider, on the other hand, that recent ab-initio molecular dynamic calculations demonstrated a tendency of the MA cations in the $\beta$ phase to align along specific directions, in connection with the formation of strong hydrogen bond interactions with the inorganic framework,[52] which should result in possible local ferroelectric domains. Now, it is hard to estimate quantitatively the polarization of $MAPbI_3$ at room temperature but the present work sets an upper limit to the spontaneous polarization of the ferroelectric phase at 4.42 $\mu C/\mathrm{cm}^2$ at 180 K (not 38 $\mu C/\mathrm{cm}^2$ as previously reported[40]) and thus it suggests that the actual polarization of an eventual ferroelectric phase at room temperature is probably very small, only few $\mu C/\mathrm{cm}^2$. For this reason, a possible positive effect due to the the permanent polarization on the photovoltaic working mechanism of $MAPbI_3$ perovskite should not be excluded but it should be carefully considered in light of the small polarization value.

A methodological comment is in order. We have not considered different exchange-correlation functionals to take into account weak-interactions. Although an appropriate van der Waals functional could in principle slightly change the absolute value of the polarization, as we considered previously for the Grimme correction, we expect the main results presented in this work to be robust and independent from the specific functional used. However, further work is required to estimate the effects of different functionals, including different van der Waals functionals, on the FE polarization in halides, as done in Ref. 23, 24, and 63

AUTHOR INFORMATION

**Corresponding Author**

*E-mail: alessandro.stroppa@spin.cnr.it.

Tel. : +39 0862 433759. Fax: +39 0862 433033

**Notes** The authors declare no competing financial interest.

ACKNOWLEDGMENTS

The research leading to these results has received funding to CQ and FDA from the European Union Seventh Framework Programme [FP7/ 2007-2013] under Grant Agreement No. 604032 of the MESO project. A.S. would like to thanks Dr. I. Baburin (TU Dresden) for useful discussions. A.S. thanks Prof. Wua Wu for the kind invitation at Fudan University (October 2014) where this work was partially done.

*Supporting Information Available*

Mulliken population analysis has been performed. This information is available free of charge via the Internet at http://pubs.acs.org/

---

* alessandro.stroppa@spin.cnr.it

[1] Kojima, A.; Teshima, K.; Shirai, Y.; Miyasaka, T. Organometal Halide Perovskites as Visible-Light Sensitizers for Photovoltaic Cells. *J. Am. Chem. Phys.* **2009**, *131*, 6050-6051.

[2] Mingzhen Liu, M; Johnston, M. B.; Snaith, H. J. Efficient planar heterojunction perovskite solar cells by vapour deposition. *Nature* **2013**, *501*, 395-398.

[3] Zhou, H.; Chen, Q.; Li, G.; Luo, S.; Song, T. B.; Duan, H.-S.; Hong, Z.; You, J.; Liu, Y.; Yang, Y. Interface engineering of highly efficient perovskite solar cells. *Science* **2014**, *345*, 542-546.

[4] Lee, M. M.; Teuscher, J.; Miyasaka, T.; Murakami, T. N.; Snaith, H. J. Efficient hybrid solar cells based on meso-superstructured organometal halide perovskites. *Science* **2012**, *338*, 463-467.

[5] Stranks, S. D.; Eperon, G. E.; Grancini, G.; Menelaou, C.; Alcocer, M. J. P.; Leijtens, T.; Herz, L. M.; Petrozza, A.; Snaith, H. J. Electron-Hole Diffusion Lengths Exceeding 1 Micrometer in an Organometal Trihalide Perovskite Absorber *Science* **2013**, *342*, 341-344.

[6] Xing, G.; Mathews, N.; Sun, S.; Lim, S. S.; Lam, Y. M.; Graetzel, M.; Mhaisalkar, S.; Sum, T. C. Long-Range Balanced Electron- and Hole-Transport Lengths in Organic-Inorganic $CH_3NH_3PbI_3$ *Science* **2013**, *342*, 344-347.

[7] Edri, E.; Kirmayer, S.; Cahen, D.; Hodes, G. High Open-Circuit Voltage Solar Cells Based on Organic-Inorganic Lead Bromide Perovskite. *J. Phys. Chem. Lett.* **2013**, *4*, 897-902.

[8] Wehrenfennig, C.; Eperon, G. E.; Johnston, M. B.; Snaith, H. J.; Herz, L. M. High Charge Carrier Mobilities and Lifetimes in Organolead Trihalide Perovskites. *Adv. Mater.* **2014**, *26*, 1584-1589.

[9] Im, J.-H.; Lee, C.-R.; Lee, J.-W.; Park, S.-W.; Park, N.-G. 6.5% efficient perovskite quantum-dot-sensitized solar cell. *Nanoscale* **2011**, *3*, 4088-4093.

[10] Etgar, L.; Gao, P.; Xue, Z.; Peng, Q.; Chandiran, A. K.; Liu, B.; Nazeeruddin, Md. K.; Graetzel, M. Mesoscopic $CH_3NH_3PbI_3/TiO_2$ Heterojunction Solar Cells. *J. Am. Chem. Soc.* **2012**, *134*, 17396-17399.

[11] Abrusci, A.; Stranks, S. D.; Docampo, P.; Yip, H.-L.; Jen, A. K.- Y.; Snaith, H. J. High-Performance Perovskite-Polymer Hybrid Solar Cells via Electronic Coupling with Fullerene Monolayers. *Nano Lett.* **2013**, *13*, 3124-3128.

[12] Burschka, J.; Pellet, N.; Moon, S-J.; Humphry-Baker, R.; Gao, P.; Nazeeruddin, M. K.; Graetzel, M. Sequential deposition as a route to high-performance perovskite-sensitized solar cells. *Nature* **2013**, *499*, 316-319.

[13] Giorgi, G.; Yamashita, K. Organic-inorganic halide perovskites: an ambipolar class of materials with enhanced photovoltaic performances. *J. Mater. Chem. A* **2015**, *3*, 8981-8991.

[14] Giorgi, G., Fujisawa, J.-I., Segawa, H., Yamashita, K. Cation Role in Structural and Electronic Properties of 3D OrganicInorganic Halide Perovskites: A DFT Analysis. *J. Phys. Chem. C* **2014**, *118*, 12176-12183.

[15] Giorgi, G., Fujisawa, J.-I., Segawa, H., Yamashita, K. Small Photocarrier Effective Masses Featuring Ambipolar Transport in Methylammonium Lead Iodide Perovskite: A Density Functional Analysis *J. Phys. Chem. Lett.* **2013**, *4*, 4213-4216.

[16] Yin, W.-J., Yang, J.-H., Kang, J., Yan, Y., Wei, S-H. Halide perovskite materials for solar cells: a theoretical review *J. Mater. Chem. A* **2015**, *3*, 8926-8942.

[17] Luo, S., Daoud, W. A. Recent progress in organic-inorganic halide perovskite solar cells: mechanisms and material design. *J. Mater. Chem. A* **2015**, *3*, 8992-9010.

[18] Butler, K. T., Frost, J. M., Walsh, A. Ferroelectric materials for solar energy conversion: photoferroics revisited *Energy Environ. Sci.* **2015**, *8*, 838-848.

[19] Walsh, A. Principles of Chemical Bonding and Band Gap Engineering in Hybrid OrganicInorganic Halide Perovskites. *J. Phys. Chem. C Nanomater Interfaces* **2015**, *119*, 5755-5760.

[20] Filippetti, A.; Mattoni, A. Hybrid perovskites for photovoltaics: Insights from first principles.

*Phys. Rev. B* **2014**, *89*, 125203.

[21] Filippetti, A.; Delugas, P.; Mattoni, A. Radiative Recombination and Photoconversion of Methylammonium Lead Iodide Perovskite by First Principles: Properties of an Inorganic Semiconductor within a Hybrid Body. *J. Phys. Chem. C* **2014**, *43*, 24843-24853.

[22] Filip, M. R.; Giustino, F. GW quasiparticle band gap of the hybrid organic-inorganic perovskite $CH_3NH_3PbI_3$: Effect of spin-orbit interaction, semicore electrons, and self-consistency *Phys. Rev. B* **2014**, *24*, 245145.

[23] Egger, D. A.; Kronik, L. Role of Dispersive Interactions in Determining Structural Properties of Organic-Inorganic Halide Perovskites: Insights from First-Principles Calculations *J. Phys. Chem. Lett.* **2014**, *5*, 2728-2733.

[24] Lee, J.-H; Bristowe, N. C.; Bristowe, P. D.; Cheetham, A. K.
Role of hydrogen-bonding and its interplay with octahedral tilting in $CH_3NH_3PbI_3$. *Chem. Commun.* **2015**, *51*, 6434-6437.

[25] Umari, P; Mosconi, E.; De Angelis, F. Relativistic GW calculations on $CH_3NH_3PbI_3$ and $CH_3NH_3SnI_3$ Perovskites for Solar Cell Applications *J. Phys. Chem. Lett.* **2014**, *5*, 2728-2733.

[26] Stroppa, A.; Jain, P; Barone, P.; Marsman, M.; Perez-Mato, J. M.; Cheetham, A. K.; Kroto, H. W.; Picozzi, S. Electric Control of Magnetization and Interplay between Orbital Ordering and Ferroelectricity in a Multiferroic Metal-Organic Framework. *Angew. Chem Int. Edit.* **2011**, *50*, 5847-5850.

[27] Stroppa, A.; Barone, P.; Jain, P.; Perez-Mato, J. M.; Picozzi, S. Hybrid Improper Ferroelectricity in a Multiferroic and Magnetoelectric Metal-Organic Framework. *Adv. Mat.* **2013**, *25*, 2284.

[28] Di Sante, D.; Stroppa, A.; Jain, P.; Picozzi, S. Tuning the Ferroelectric Polarization in a Multiferroic Metal-Organic Framework. *J. Am. Chem. Soc.* **2013**, *135*, 18126-18130.

[29] Gaussian 09, Revision D.01, Frisch, M. J.; Trucks, G. W.; Schlegel, H. B.; Scuseria, G. E.; Robb, M. A.; Cheeseman, J. R.; Scalmani, G.; Barone, V.; Mennucci, B.; Petersson, G. A.; Nakatsuji, H.; Caricato, M.; Li, X.; Hratchian, H. P.; Izmaylov, A. F.; Bloino, J.; Zheng, G.; Sonnenberg, J. L.; Hada, M.; Ehara, M.; Toyota, K.; Fukuda, R.; Hasegawa, J.; Ishida, M.; Nakajima, T.; Honda, Y.; Kitao, O.; Nakai, H.; Vreven, T.; Montgomery, J. A., Jr.; Peralta, J. E.; Ogliaro, F.; Bearpark, M.; Heyd, J. J.; Brothers, E.; Kudin, K. N.; Staroverov, V. N.; Kobayashi, R.; Normand, J.; Raghavachari, K.; Rendell, A.; Burant,

J. C.; Iyengar, S. S.; Tomasi, J.; Cossi, M.; Rega, N.; Millam, J. M.; Klene, M.; Knox, J. E.; Cross, J. B.; Bakken, V.; Adamo, C.; Jaramillo, J.; Gomperts, R.; Stratmann, R. E.; Yazyev, O.; Austin, A. J.; Cammi, R.; Pomelli, C.; Ochterski, J. W.; Martin, R. L.; Morokuma, K.; Zakrzewski, V. G.; Voth, G. A.; Salvador, P.; Dannenberg, J. J.; Dapprich, S.; Daniels, A. D.; Farkas, O.; Foresman, J. B.; Ortiz, J. V.; Cioslowski, J.; Fox, D. J. Gaussian, Inc., Wallingford CT, 2009..

[30] Tian, Y.; Stroppa, A.; Chai, Y.-S.; Barone, P.; Perez-Mato, M.; Picozzi, S.; Sun, Y. High-temperature ferroelectricity and strong magnetoelectric effects in a hybrid organic-inorganic perovskite framework. *Phys. Status Solidi RRL* **2015**, *9*, 62-67.

[31] Tian, Y.; Stroppa, A.; Chai, Y.-S.; Yan, L.; Wang, S.; Barone, P.; Picozzi, S.; Sun, Y. Cross coupling between electric and magnetic orders in a multiferroic metal-organic framework. *Sci. Rep.* **2014**, *4*, 6062.

[32] Jain, P.; Ramachandran, V.; Clark, R. J.; Zhou, H. D.; Toby, B. H.; Dalal, N. S., Kroto, H. W.; Cheetham, A. K. Multiferroic behavior associated with an order-disorder hydrogen bonding transition in metal-organic frameworks (MOFs) with the perovskite $ABX_3$ architecture. *J. Am. Chem. Soc.* **2009**, *131*, 13625-7.

[33] Poglitsch, A.; Weber, D. Dynamic disorder in methylammoniumtrihalogenoplumbates (II) observed by millimeterwave spectroscopy. *J. Chem. Phys.* **1987**, *87*, 6373-6378.

[34] Onoda-Yamamuro, N.; Matsuo, T.; Suga, H. Calorimetric and IR spectroscopic studies of phase transitions in methylammonium trihalogenoplumbates(II). *J. Phys. Chem. Solids* **1990**, *51*, 1383-1395.

[35] Onoda-Yamamuro, N.; Matsuo, T.; Suga, H. Dielectric study of $CH_3NH_3PbX_3$ (X = Cl, Br, I). *J. Phys. Chem. Solids* **1992**, *53*, 935-939.

[36] Coll, M.; Gomez, A.; Mas-Marza, E.; Almora, O.; Garcia-Belmonte, G.; Campoy-Quile, M.; Bisquer, J.

Polarization Switching and Light-Enhanced Piezoelectricity in Lead Halide Perovskites.

*J. Phys. Chem. Lett.* **2015**, *6*, 1408-1413.

[37] Gesi, K. Effect of hydrostatic pressure on the structural phase transitions in $CH_3NH_3PbX_3$ (X =Cl, Br, I). *Ferroelectrics* **1997**, *203*, 249-268.

[38] Stoumpos, C. C.; Malliakas, C. D.; Kanatzidis, M. G. Semiconducting Tin and Lead Iodide Perovskites with Organic Cations: Phase Transitions, High Mobilities, and Near-Infrared Pho-

toluminescent Properties. *Inorg. Chem.* **2013**, *52*, 9019-9038.

[39] Beilsten-Edmands, J.; Eperon, G. R.; Johnson, R. D.; Snaith, H. J.; Radaelli, P. G. Non-ferroelectric nature of the conductance hysteresis in CH3$NH_3PbI_3$ perovskite-based photovoltaic devices *Appl. Phys. Lett.* **2015**, *106*, 173502.

[40] Frost, J. M.; Butler, K. T.; Brivio, F.; Hendon, C. H.; van Schilfgaarde, M.; Walsh, A. Atomistic Origins of High-Performance in Hybrid Halide Perovskite Solar Cells. *Nano Lett.* **2014**, *14*, 2584-2590.

[41] Wieder, H. H. Electrical Behavior of Barium Titanatge Single Crystals at Low Temperatures. *Phys. Rev.* **1955**, *99*, 1161-1165.

[42] Dall'olio, S.; Dovesi, R.; Resta, R. Spontaneous polarization as a Berry phase of the Hartree-Fock wavefunction: The case of $KNbO_3$. *Phys. Rev. B* **1997**, *56*, 10105-10114.

[43] Yang, S. Y.; Seidel, J.; Byrnes, S. J.; Shafer, P.; Yang, C.-H.; Rossell, M. D; Yu, P.; Chu, Y.-H.; Scott, J. F.; Ager III, J. W.; Martin, L. W.; Ramesh, R. Above-bandgap voltages from ferroelectric photovoltaic devices. *Nature Nanotechnology* **2010**, *5*, 143-147.

[44] Frost, J. M.; Butler, K. T.; Walsh, A. Molecular ferroelectric contributions to anomalous hysteresis in hybrid perovskite solar cells. *APL Mater.* **2014**, *2*, 081506.

[45] Quarti, C.; Mosconi, E.; De Angelis, F. Interplay of Orientational Order and Electronic Structure in Methylammonium Lead Iodide: Implications for Solar Cells Operation. *Chem. Mater.* **2014**, *26*, 6557-6569.

[46] Zheng, F.; Takenaka, H.; Wang, F.; Koocher, N. Z.; Rappe, A. M. First-Principles Calculation of the Bulk Photovoltaic Effect in $CH_3NH_3PbI_3$ and $CH_3NH_3PbI_{3-x}Cl_x$. *J. Phys. Chem. Lett.* **2015**, *6*, 31-37.

[47] Stroppa, A.; Di Sante, D.; Barone, P.; Bokdam, M.; Kresse, G.; Franchini, C.; Whangbo, M.-H. Picozzi, S. Tunable ferroelectric polarization and its interplay with spinorbit coupling in tin iodide perovskites. *Nature Comm* **2014**, *5*, 3335-3339.

[48] Kutes, Y.; Ye, L.; Zhou, Y.; Pang, S.; Huey, B. D.; Padture, N. P. Direct Observation of Ferroelectric Domains in Solution-Processed $CH_3NH_3PbI_3$ Perovskite Thin Films *J. Phys. Chem. Lett.* **2014**, *5*, 3335-3339.

[49] Liu, S.; Zheng, F; Koocher, N. Z.; Takenaka, H.; Wang, F.; Rappe, A. M. Ferroelectric Domain Wall Induced Band Gap Reduction and Charge Separation in Organometal Halide Perovskites. *J. Phys. Chem. Lett.* **2015**, *6*, 693-699.

[50] Cohen, R. E. Origin of ferroelectricity in perovskite oxides. *Nature* **1992**, *358*, 136-138.

[51] Amat, A.; Mosconi, E.; Ronca, E.; Quarti, C.; Umari, P.; Nazeeruddin, Md. K.; Grtzel, M.; De Angelis, F. Cation-Induced Band-Gap Tuning in Organohalide Perovskites: Interplay of SpinOrbit Coupling and Octahedra Tilting *Nano Lett.* **2014**, *14*, 3608-3616.

[52] Quarti, C.; Mosconi, E.; De Angelis, F. Structural and electronic properties of organo-halide hybrid perovskites from ab initio molecular dynamics *Phys. Chem. Chem. Phys.* **2015**, *17*, 9394-9409.

[53] Perdew, J. P.; Ruzsinszky, A., Csonka, G. I.; Vydrov, O. A.; Scuseria, G. E.; Constantin, L. A., Zhou, X., Burke, K. Restoring the Density-Gradient Expansion for Exchange in Solids and Surfaces. *Phys. Rev. Lett.* **2008**, *100*, 136406.

[54] Kresse, G.; Furthmüller, J. Efficient iterative schemes for ab initio total-energy calculations using a plane-wave basis set. *Phys. Rev. B* **1996**, **54**, 11169.

[55] Resta, R. Macroscopic polarization in crystalline dielectrics: the geometric phase approach. *Rev. Mod. Phys.* **1994**, **66**, 899.

[56] King-Smith, R. D.; Vanderbilt, V. Theory of polarization of crystalline solids. *Phys. Rev. B* **1993**, **47**, 1651.

[57] Wasylishen, R. E.; Knop, O.; Macdonald, J. B. Cation rotation in methylammonium lead halides. *Solid State Commun.* **1985**, *56*, 581-582.

[58] Quarti, C.; Grancini, G.; Mosconi, E.; Bruno, P.; Ball, J. M.; Lee, M. M.; Snaith, H. J.; Petrozza, A.; De Angelis, F. The Raman Spectrum of the $CH_3NH_3PbI_3$ Hybrid Perovskite: Interplay of Theory and Experiment. *J. Phys. Chem. Lett.* **2014**, *5*, 279-284.

[59] Mosconi, E.; Quarti, C.; Ivanovska, T.; Ruani, G.; De Angelis, F. Structural and electronic properties of organo-halide lead perovskites: a combined IR-spectroscopy and *ab initio* molecular dynamics investigation. *J. Phys. Chem. Lett.* **2014**, *16*, 16137-16144.

[60] Zhang, Q.; Cagin, T.; Goddard, W. A. The ferroelectric and cubic phases in $BaTiO_3$ ferroelectrics are also antiferroelectric. *Proc. Natl. Acad. Sci. U.S.A.* **2006**, *103*, 14695-14700.

[61] Weller, M. T.; Weber, O. J.; Henry, P. F.; Di Pumpo, A. M., Hansen, T. C. Complete structure and cation orientation in the perovskite photovoltaic methylammonium lead iodide between 100 and 352 K. *Chem. Commun.* **2015**, *51*, 4180-4183.

[62] Grimme, S. Accurate description of van der Waals complexes by density functional theory including empirical corrections *J. Comput. Chem.* **2004**, *25*, 1463-1473.

[63] Di Sante, D.; Stroppa, A., Picozzi, S. Structural, electronic and ferroelectric properties of croconic acid crystal: a DFT study. *Phys. Chem. Chem. Phys.* **2012**, *14*, 14673-14681.

# Supplementary Material

Alessandro Stroppa,[1] Claudio Quarti,[2] Filippo De Angelis,[2] and Silvia Picozzi[1]

[1] *CNR-SPIN, 67100 L'Aquila, Italy**

[2] *Computational Laboratory for Hybrid/Organic Photovoltaics (CLHYO), CNR-ISTM, 06123 Perugia Italy*

## I. CHARGE ANALYSIS OF METHYLAMMONIUM CATION

The MA cation is formed by a $NH_3$ and $CH_3$ group though a C-N bond. By following a Lewis rapresentation of the MA group, and by computing the formal charges, as known by standard inorganic text-books, one ends up with $\delta_C$=0 and $\delta_N$=+1, (where $\delta$ represents the formal charge on the corresponding atom) thus suggesting a net charge on the $NH_3$ group.

To verify this assumption, Mulliken population analysis has been carried out on methylammonium $CH_3NH_3^+$ cation with the Gaussian 09 code, at a similar level of theory with respect to that used in the periodic calculations (PBE exchange-correlation functional + 6-311G(d,p) basis set). The present analysis provides the following results: the Mulliken charge on C is $-0.2522$ and that on its H atoms is 0.2094; the Mulliken charge on N is $-0.3265$ and that on its H atoms is 0.3168. The sum of Mulliken atomic charges is normalized to 1. When the Mulliken charges with hydrogens are summed into heavy atoms one obtains: 0.3761 for C and 0.6239 for N thus suggesting that the 62% of the positive charge is located mainly on the $NH_3$ group. In particular one finds that the hydrogen bonded to the nitrogen are significantly more positive than those bonded to the carbon.

In order to confirm this picture, we have carried out the same analysis also with the more involved Hirshfeld scheme for the atomic population analysis. The results of this analysis, confirm the previous picture, predicting an enhancement of the positive charge localization on the $NH_3$ group. The Hirshfeld charges with hydrogens summed into heavy atoms are 0.3 and 0.7 for C and N respectively.